Condensing CNNs with Partial Differential Equations

Anil Kag, Venkatesh Saligrama
Department of Electrical and Computer Engineering, Boston University
{anilkag, srv}@bu.edu

Abstract

Convolutional neural networks (CNNs) rely on the depth of the architecture to obtain complex features. It results in computationally expensive models for low-resource IoT devices. Convolutional operators are local and restricted in the receptive field, which increases with depth. We explore partial differential equations (PDEs) that offer a global receptive field without the added overhead of maintaining large kernel convolutional filters. We propose a new feature layer, called the Global layer, that enforces PDE constraints on the feature maps, resulting in rich features. These constraints are solved by embedding iterative schemes in the network. The proposed layer can be embedded in any deep CNN to transform it into a shallower network. Thus, resulting in compact and computationally efficient architectures achieving similar performance as the original network. Our experimental evaluation demonstrates that architectures with global layers require $2-5\times$ less computational and storage budget without any significant loss in performance.

1. Introduction

Convolutional neural networks (CNNs) have been the backbone for recent advances in image recognition [19], object detection [33], and other applications [31] interfacing the image modalities. Convolutional filters with limited receptive fields act on localized input regions to generate low-level features. Features used for decision-making are complex functions of these low-level features, achieved through the composition of many such convolutional operators applied in sequence, resulting in deep networks with high inference/train time and large model size.

Recent works [3, 5] have explored neural networks inspired by ordinary differential equations (ODEs), offering richer representation than their discrete counterparts. Resnets [8] can be viewed as a discretized form of ODEs. The final architecture based on these continuous layers leads to higher computational cost in comparison to their discrete counterpart [2], namely due to the costly fixed point solvers. In contrast, we explore novel constraints on the feature maps, based on partial differential equations (PDEs) that offer similar rich representation but with shallower neural networks. In addition, we provide efficient and scalable solvers to provide computational and storage savings.

Proposed Method. We explore a hybrid approach wherein we modify discrete models by embedding a new layer with a global receptive field that operates on the input feature map and computes complex compositions of these low-level features. We call this layer the Global feature layer. It approximately solves a PDE constraint that couples the input and output feature maps. In a typical discrete model, at every input resolution, the same convolutional block is applied repeatedly m times. We modify this structure by keeping only one convolutional block and replacing the $m-1$ blocks with a single global feature layer (see Figure 1). Thus, reducing the deep neural network to a much shallower network without any significant performance loss. It leads to smaller models with low computational and storage costs. In addition, it improves both the train and inference times.

By keeping at least one block from the original architecture, we are incorporating the signature of this architecture. It allows the application of this generic global feature layer to any architecture. Also, since a good start for any iterative solver implies smaller steps to reach the solution, this original block helps to initialize the PDE solution.

Estimated Savings. Suppose a Resnet architecture constructed with three resolutions has m residual blocks, and for the three resolutions, the compute cost is $= \{c_1, c_2, c_3\}$ respectively. The total compute cost for operating this network is $m \times (c_1 + c_2 + c_3)$. Global residual block replaces $m-1$ residual blocks with just one global block and assuming that the cost of this global block is similar, i.e. $= \{c_1, c_2, c_3\}$, then the cost to operate the modified network is $2 \times (c_1 + c_2 + c_3)$. Given that $m > 2$, the modified network can lead to computational savings over Resnet. Similar conclusions can be drawn for storage savings.

Motivational Example. To motivate our approach, we apply the Global feature layer to the Resnet32 [8] architecture, where at each feature map resolution, the same block repeats 5 times. With the experimental setup described in the section 4, we train three models on the CIFAR-10 dataset: (a)

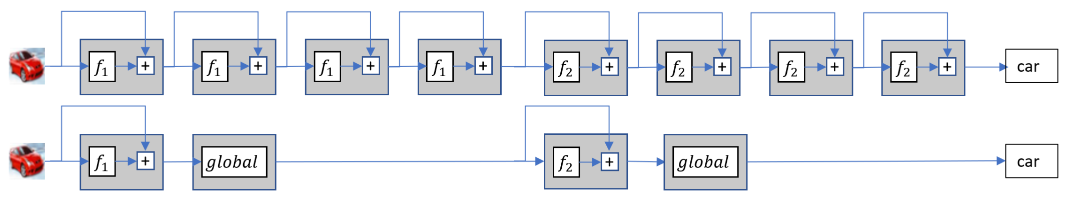

Figure 1. Replacing repeated blocks in a given CNN architecture with the Global layer for compute and model savings.

Resnet32 : same architecture as used in [8], (b) ODE based Resnet32, i.e., MDEQ [2] modified to match feature map configuration as in Resnet32, and (c) ResNet32-Global : replaced repeated blocks with global layers. Table 1 shows that both Resnet32 and MDEQ have similar performance. Note that MDEQ is significantly costly in terms of the floating-point multiply-add operations (MACs). In contrast, the proposed Resnet32-Global results in a much smaller model and a significantly lower computational footprint without any hit in the performance. This experiment clearly shows that the Global layer results in the following benefits:

1. **Shallow network.** Resnet32-Global has $\approx 3\times$ less depth.
2. **Less storage.** Resnet32-Global has $\approx 3\times$ less parameters.
3. **Less compute.** Resnet32-Global uses $\approx 5\times$ less MACs.
4. **Readily embedable in any network.**

Table 1. CIFAR-10 : Comparison between discrete Resnet32, ODE based Resnet32 (MDEQ [2]), and our PDE embedded Resnet32-Global. We compute the depth as the number of blocks in the network. Train and Inference time denote the cost of processing one pass of the train and test dataset on a V100 GPU. Supplementary Table 16 lists results for Resnet ($m = 2$) and CIFAR-100 dataset.

	Accuracy	**#Params**	**#MACs**	**Train Time(s)**	**Inference Time(s)**	**Depth**
Resnet32	92.49%	460K	70M	78	4.45	15
MDEQ	92.28%	1.1M	1.5B	409	23.32	-
Resnet32-Global	91.93%	162K	15M	24	1.91	6

Contributions.

- Proposed a Global feature layer that imposes PDE constraints on the input and output feature maps. Embedding this layer in deep networks results in their shallower variants with a smaller footprint with similar performance.
- Embedded the proposed global layer in many existing CNN architectures and conducted an extensive empirical study on benchmark image recognition datasets to show computational and storage savings.
- Proposed an efficient and approximate PDE solver to embed in the neural network wherein model accuracy can be traded-off for the computational budget.
- We provide pseudo-code for the Global layer that is readily deployable in any popular deep learning library. Our PyTorch implementation is available at https://github.com/anilkagak2/PDE_GlobalLayer.

2. Related Work

There is a vast literature related to models for object recognition, including low complexity models. Here we only include papers closely related to our approach.

Early Skip CNNs. Resnet [8], Highway networks [27], Wide-Resnets [32], Dense-Nets [12], etc. proposed networks with skip/residual connections. These changes helped alleviate the vanishing gradient issues in the deep neural networks. These trained much deeper models and hence achieved significantly better performance than the previous generation models like AlexNet [19], VGG-Nets [26], etc. Note that deeper models implicitly mean larger storage costs and higher compute requirements.

Mobile/IoT ready CNNs. Many initial attempts (SqueezeNet [14], SqueezeNext [6], MobileNets [11]) at designing low complexity models included handcrafted feature blocks (with low rank filters, separable convolutions, etc.) whose composition yielded small models with low floating-point operations. Recently, EfficientNets [29] were proposed to systematically study the effect of width, depth, channels, etc., along with memory and MACs constraints. There have also been efforts [21, 34] to search for neural architectures that outperform hand-crafted architectures. Note that these are complementary to our proposal.

Model Compression/Distillation. An alternate strategy to obtain small models require model compression. Deep-compression [7] is an early work where a pre-trained network is pruned, quantized, and compressed to yield small networks which can be deployed on the edge devices. Other works include distilling [9] knowledge from a larger pre-trained network into a small compact model. We do not pursue these techniques to simplify our exposition.

ODE Inspired CNNs. Related work in this class has the most similarity with our approach. Neural ODEs (NODEs) [3] introduce continuous time layers following an ODE. It uses black-box ODE solvers along with the adjoint method for back-propagation. Augmented Neural ODEs [4] extend NODEs to a richer class of functions while ANODE [5] addresses the gradient computation in the adjoint method to allow for more accurate gradients matching the discretization. Neural ODEs and their variants do not demonstrate their scalability to tasks like Imagenet.

There have been previous works that utilize ODE-inspired models for sequential processing. Some of these models require the architecture to achieve equilibrium [15, 17], [1], where the later has been extended to image modalities by Multi-scale deep equilibrium models (MDEQs) [2]. MDEQs use implicit layers at multiple feature scales to scale to large datasets such as Imagenet. Although they show good performance on large-scale tasks, the model capacity still needs to be nearly the same as the discrete counterparts. Although implicit models offer low memory cost training, they still do not offer much flexibility for inference. In addition, their inference cost is much higher in comparison to discrete variants such as Resnet.

PDE Inspired CNNs. [24] proposed new architectures based on parabolic and hyperbolic partial differential equations. These connections with PDEs enable theoretical reasoning, such as the stability of the resulting network. Although the resulting models are small, these models take a significant hit in performance. NeuPDE [28] uses the convolutional filters to approximate the differential operators for generic second order PDE. NeuPDEs downsample the input image to a manageable feature map through many convolutional layers and then finally applies the PDE blocks. This construction helps in reducing the model size but the gains are not sufficient enough.

3. Method

In this section, we will formalize the PDE constraint on the feature representation. We will describe the proposed Global layer, including our PDE choice, and embed an approximate numerical solver in the neural network. Finally, we will provide building blocks and pseudo-code to improve the understanding of our architecture.

Notation. For simplicity, we will assume that the output shape is the same as the input, and we are dealing with only a $2D$ feature map represented by the $X - Y$ plane. Let $I(x, y) \in \mathbb{R}^{h\times w}$ denote the input feature map with $h \times w$ entries. Let $H(x, y) \in \mathbb{R}^{h\times w}$ be the output feature map. We will denote Δ_{xy} as the differential operator (contains partial differential operators for various interactions between the two dimensions in the input).

3.1. PDE Constrained Features.

We enforce the following PDE constraint on the output feature map H

$$\Delta_{xy} H(x, y) = f(I(x, y)) \tag{1}$$

where f is a function applied on the input feature map. The above operator applies globally on the feature map and does not restrict itself to the local receptive field of operators such as one-layer convolutions.

Illustration. Before delving into further details about the global feature layer (namely the exact PDE and the numerical solver), we provide an intuitive example on the MNIST dataset to demonstrate the effectiveness of such a strategy. We construct a network with one feature layer followed by average pooling operation and classifier layer (see Figure 2). Note that the feature map layer constructs only one feature map. It gives rise to three networks by using different feature layers : (a) CNN-Net: convolutional layer as the feature map, (b) Residual-Net: a residual connection between the convolutional layers, and (c) PDE-Net: PDE constrained layer as the feature map. Note that all three networks have 524 parameters to ensure a fair comparison. Thus the only difference between these networks remains in the way features are processed. We train these networks on the MNIST dataset with the same settings (optimizer, learning rate, epochs, no data-augmentations, see Sec. 4) to provide a fair evaluation.

On the held-out test set, CNN-Net achieves 92.01% accuracy, Residual-Net achieves 92.53% accuracy, while PDE-Net achieves 95.03% accuracy. Since the network architecture apart from the feature layer is the same, we can analyze the feature map easily to see the contrast between the two feature representations. Figure 2 shows the intermediate representation from these neural networks. It shows that the feature maps generated by PDE-Net effectively highlight the input object by smoothing the noisy background and increasing brightness around the object edges.

3.2. Global Feature Layer

To embed a PDE in the neural network layer, we need to describe four components of the PDE: (a) its exact form, i.e. Δ_{xy}, (b) a numerical solver, (c) initial guess of the solution, and finally (d) choice of free parameters such as the function

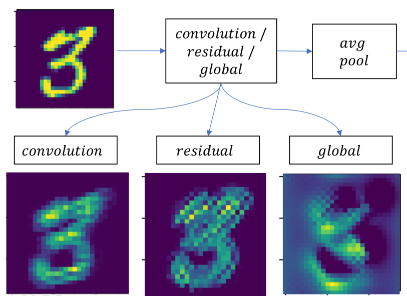

Feature Backbone	Acc. (%)	Confusion b/w 3 & 5
Convolution	92.01	27
Residual	92.53	30
Global	**95.03**	**9**

Figure 2. Toy Example comparing different backbones: Convolutional, Residual, and Global. We show network representation for the input image for the letter three. Intermediate features from Convolutional and Residual backbones do not show bright intensity around the edges and have an uneven background. In contrast, the Global layer smoothens it out and shows bright spots around the digit. Thus, the Global layer provides a better and markedly different representation than the other two backbones. All three networks have 524 parameters. Network with Global layer achieves 95% accuracy while the other two achieves $\approx 92.5\%$ accuracy. It also has a significantly lesser confusion between the letters 3 and 5. See other visualizations in supplementary Sec. A.9.

f. We refer to this new layer as the Global feature layer and describe these components below.

(a) PDE: At the heart of the Global feature layer is the following generic advection-diffusion PDE [1]

$$\frac{\partial}{\partial t} H = \nabla \cdot (D \nabla H) + \nabla \cdot (\mathbf{v} H) + f(I) \tag{2}$$

It lets us treat the input feature map pixels as particles in motion with velocity $\mathbf{v}$ that interact with their neighborhood through diffusion coefficient D. Starting at time $t = 0$ with initial guess of the concentration $H(t = 0)$, the solution of this advection-diffusion equation provides the final particle concentration $H(t = T)$ at time T. It is the output representation of the global feature layer. The motion of the particles affects the concentration and is modelled by the *advection* term $\nabla \cdot (\mathbf{v}H)$. Similarly, the term $\nabla \cdot (D\nabla H)$ describes the *diffusion* phenomenon, where particles shift between low and high concentrations to reach a steady state. Note that both D and $\mathbf{v}$ can be a function of the particle locations. Finally, the term $f(I)$ is the source of the particle concentration.

In our 2D world, the velocity and diffusion coefficients have two components, i.e. $\mathbf{v} = (u, v)$ and $D = (D_x, D_y)$, and the Eq. 2 boils down to the following form [13]

$$\begin{aligned} &\frac{\partial}{\partial t} H(x,y,t) + \frac{\partial}{\partial x}\left(u(x,y,t)H(x,y,t)\right) + \frac{\partial}{\partial y}\left(v(x,y,t)H(x,y,t)\right) \\ &= \frac{\partial}{\partial x}\left(D_x \frac{\partial}{\partial x} H(x,y,t)\right) + \frac{\partial}{\partial y}\left(D_y \frac{\partial}{\partial y} H(x,y,t)\right) + f(I(x,y)) \end{aligned} \tag{3}$$

(b) Iterative Solver: For an efficient implementation of the global layer, we need a simple and efficient PDE solver that can be embedded in the neural network and can achieve approximate solutions easily. To obtain a finite element scheme, it is standard in the literature to expand the partial differential operators with their finite-difference elements. Assume the discrete steps for x, y and t by δ_x, δ_y and δ_t respectively. Following [13], we discretize the Eq. 3 as (see Supplementary Sec. A.2 for detailed derivation),

$$\begin{aligned} LH^{k+1}_{x,y} &= MH^{k-1}_{x,y} - 2(u_x + v_y)\delta_t H^k_{x,y} + 2\delta_t f(I(x,y)) \\ &+ (-A_x + 2B_x)H^k_{x+1,y} + (A_x + 2B_x)H^k_{x-1,y} \\ &+ (-A_y + 2B_y)H^k_{x,y+1} + (A_y + 2B_y)H^k_{x,y-1} \end{aligned} \tag{4}$$

where $L = (1 + 2B_x + 2B_y)$, and $M = (1 - 2B_x - 2B_y)$

$$u_x = \frac{u_{x+1,y} - u_{x-1,y}}{2\delta_x}; v_y = \frac{v_{x,y+1} - v_{x,y-1}}{2\delta_y};$$

$$A_x = \frac{u\delta_t}{\delta_x}; A_y = \frac{v\delta_t}{\delta_y}; B_x = \frac{D_x\delta_t}{\delta_x^2}; B_y = \frac{D_y\delta_t}{\delta_y^2};$$

[1]https://en.wikipedia.org/wiki/Convection-diffusion_equation

Given a suitable initialization of the output feature map H at $t = 0$, Eq. 4 provides an update rule to find the PDE solution at any time $t = T$. We need to initialize the algorithm and we can take K steps of this iteration on the entire 2D map to get the solution at time $T = K\delta_t$.

(c) Initialization: An initial guess of the solution is crucial for the convergence of the previous recursion. A better initial guess leads to faster convergence. Multiple strategies exist to initialize the output feature map, namely (a) input feature map I, (b) fixed function of the input, and (c) a learnable function of the input. We follow the last option. Given an architecture, we use one of its building blocks as the initialization point and learn its parameters during the training stage with back-propagation. Thus, for architecture such as Resnet, at any resolution level, we use the first block as the output of the global feature layer at $t = 0$. We run the PDE for K steps to get the final feature map at time $\frac{K}{\delta_t}$.

(d) Choice of the free parameters: There are some free parameters in the Eq. 3. To complete the description of the Global feature layer, we list our parameterization for these free parameters, namely (a) function f (b) particle velocity (u, v), and (c) diffusion coefficient (D_x, D_y). For simplicity, we keep f as identity operator on the input and learn other parameters as the depth-wise convolution over the initialization. We point out that, for compute savings, one can further fix these parameters by keeping identity operations or treating these as hyper-parameters. We study the impact of different choices for free parameters in our ablations (see Sec. 4.6 & Supplementary Sec. A.6). We leave the design choice improvements (ex. employing architectural search for better combinations) for future work.

Finally, as a passing remark, we point out that we have not handled the boundary conditions explicitly in our formulation. Ideally, one should carefully design the behavior of the PDE at the boundary. Instead, we roll the image such that the first particle is a neighbor of the last. Since our goal is only to find an approximation, this modification suffices.

Note that our choices for the PDE and the numerical solver are motivated by the ease of implementation and simplicity in exposition. We leave the exploration of various other PDEs (Laplace equations, Heat equations, Navier-Stokes etc.) and better solvers to future work.

Implementation. Algorithm 1 shows the pseudo-code for the Global layer. This feature layer integrates easily in any architecture with appropriate initializations. By default, we take the discrete step sizes to be $\delta_t = 0.2$, and run the recursions till $K = 5$ steps, resulting in the output state at $T = K\delta_t = 1$. We take $\delta_x = \delta_y = 1$ as the pixel values are not available at any finer details. For all our experiments, free parameters in Eq. 3 are depthwise convolutional operators with the same kernel size as the original block. For CIFAR-10 low-budget experiments, we use constant diffusion coefficients and set 1 as their default values.

Algorithm 1 Pseudo Code for the Global Feature Block

```
**Input :** Input feature map $I \in \mathbb{R}^{h \times w}$
**Input :** Initial solution guess $F(I)$, Function $f$
**Output :** Output feature map $O$
**Init :** $H^{-1} = H^0 = F(I)$
Compute velocity $(u, v)$, diffusion coefficient $(D_x, D_y)$
**for** $k = 1$ **to** $K$ **do**
  Compute $f(H^{k-1}, I)$
  **for** $x = 1, y = 1$ **to** $h, w$ **do**
    Set $H^{k+1}[x, y]$ as per Eq. 4
  **end for**
  Set output feature map $O = H^K$
**end for**
```

Differences from existing PDE/ODE CNNs. Existing ODE-based CNNs [3] have focused on showing an equivalence between Resnet like architectures and the continuous-time ODEs. Although such connections provide new insights, few efforts utilize such ideas for compact CNNs due to expensive fixed point solvers and costly residual functions. Thus, these architectures are unable to scale-up to large datasets such as Imagenet (see Supplementary Sec. A.8 for further details).

Existing PDE-based CNNs [24, 28] apply generic stencil operators and do not solve any specific PDE. Furthermore, most of the works use such operators on the heavily down-sampled initial feature map. In contrast, we apply the proposed Global layer at every resolution level and remove the dependence on the repetition of the architectural blocks.

We also point out that our update Eq. 4 is not a simple residual connection. It is a discretization corresponding to the PDE Eq. 3, wherein different elements interact in time and spatial dimensions. In contrast, a recursive update of any generic convolution would not necessarily correspond to an iterative scheme and will not converge. In addition, we do not have expensive non-linearities in the update equation that slow down the recursion. Typically in ODE/PDE CNNs, the function f is a residual block with multiple full convolutions and non-linearities like batch-norm and activation functions.

Architectures with Global layer. Fig. 3 shows an schematic of the proposed Global layer. As discussed earlier, the free parameters in this layer are constructed as depthwise convolutions. This layer can be embedded in any existing architectures as seen in Sec. 4.

4. Experiments

In this section, we will apply the proposed Global layer in popular architectures. We will show that the resulting architectures have a much smaller computational and storage footprint than the original models. We will evaluate these models on various benchmark image recognition datasets.

4.1. Datasets

We use popular image classification datasets to show that our architectures provide benefits across many tasks. These datasets are publicly available. Our models are trained from scratch using the available training data. We report evaluation metrics on the publicly available test set.

1. **MNIST-10** [20] : This dataset consists of 10 classes with grayscale images of 28×28 pixels. There are $60,000$ images in the training set and $10,000$ images in the test set. We normalize the data to be mean 0 and variance 1.
2. **CIFAR-10/100** [18] : This dataset consists of RGB images of 32×32 pixels. It contains $50,000$ training and $10,000$ test images. It has two variants: (a) CIFAR-10 images are drawn from 10 classes, and (b) CIFAR-100 images are drawn from 100 classes. Unless explicitly stated, we follow standard data augmentation techniques (mirroring/shifting) used in earlier works [8, 12], followed by normalization to a standard gaussian across channels.
3. **Imagenet-1000** [23] : It is the popular ILSVRC 2012 classification dataset. This 1000 way classification dataset consists of 1.28 million training and $50,000$ validation images. We follow the standard data augmentation (mirroring, resize and crop to shape 224×224) for training and single crop for testing. Similar to previous works, we report results on the validation set.

4.2. Experimental Setup

We implement the Global feature layer in PyTorch using the Algorithm 1. Our experiments include strong baselines such as Resnet [8], Densenet [12], Wide Resnet [32], DARTS [22]. We embed global feature layers in these architectures and remove feature block repetitions resulting in Resnet-Global, Densenet-Global, Wide Resnet-Global, and DARTS-Global. For the Imagenet experiments, we perform similar adjustments to the state-of-the-art architectures such as MobileNetV3 [10] and EfficientNet [29]. We follow guidance from these works for a fair comparison. Unless the original papers recommend extra augmentation or training techniques, we minimize cross-entropy loss with the stochastic gradient descent with momentum optimizer in all our experiments. In addition, we cite known results from the literature for baseline reference.

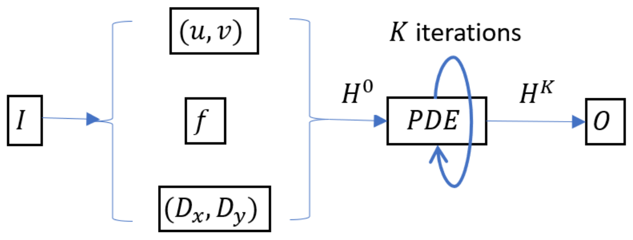

Figure 3. Schematic for the Global layer using the diffusion PDE.

We primarily report accuracy, the number of parameters, and the number of floating-point multiply-add operations[2]. These metrics measure the performance, model size, and computational footprint of a model. Due to lack of space, we tabulate depth, inference, and training times for only a few experiments. We do not pursue compression-related ideas (quantization, deep-compression, distillation, etc.) or hardware optimizations in this work to simplify the crux of our exposition. These can be further incorporated in our scheme to provide similar gains as reported in earlier works.

4.3. Results on MNIST-10

Since the ODE baselines do not scale to large-scale datasets, we compare our architectures with these baselines on MNIST-10 dataset. We use the Resnet architecture in this experiment. Similar to [3, 28], we use one Resnet architecture where we apply one Global or one ODE layer or 6 residual layers after downsampling the input twice. In addition, we use a budget ($<$ 5M MACs) Resnet architecture where we apply one Global layer or residual layers without downsampling (see Supplementary Sec. A.3 for details). We minimize the cross-entropy loss using the SGD optimizer with momentum. We follow a similar experimental setup (epochs, learning rate, scheduler, etc.) as the baselines.

Results. *Resnet-Global at same accuracy has* $3-5\times$ *storage gains (number of parameters) and* $2.5-3\times$ *compute gains.* Table 2 compares the Resnet-Global model with Neural ODEs [3], NeuPDE [28], Resnet [8]. It shows that Resnet-Global achieves similar performance as the baselines while reducing the number of parameters and the compute requirements. In particular, compared to Resnet, our architectures reduce the storage by $3-4\times$ and reduce the compute by $2-3\times$. On the other hand, Neural-ODEs have $3\times$ higher compute footprint when compared to Resnet.

Table 2. Results on MNIST-10. Networks with a Global layer have significantly less storage and compute requirements than ODE, PDE, and discrete CNNs.

Architecture	Accuracy	#Params	#MACs
Neural ODEs [3]	99.49	220K	100M
NeuPDE [28]	99.49	180K	
Resnet [3, 8]	99.59	600K	30M
Resnet-Global (ours)	99.51	136K	14M
Resnet	99.61	33.3K	5.7M
Resnet-Global (ours)	99.43	9.94K	1.7M

4.4. Results on CIFAR-10 & CIFAR-100

Architectures. We evaluated popular residual architectures in this task, namely Resnet, Wide-Resnets, and DenseNets. We ran two variants of Resnet [8]: Resnet32 repeats same residual block $m = 5$ times at every resolution while Resnet56 increases the repetitions to $m = 9$. We strictly adhere to the configuration described in the original paper [8]. We replace the repeated blocks in these architectures with the Global layer, resulting in two Resnet-Global architectures where we keep $m = 1$ and $m = 2$ repetitions.

We used Wide-Resnet [32] with 40 layers and $4\times$ the width of the residual architecture, commonly referred to as WRN-40-4. It is constructed similar to the above-described Resnet with $m = 6$ repetitions except with $4\times$ the width. We replace these repetitions with a Global layer, resulting in Wide-Resnet-Global with $m = 1$. For DenseNet, we borrowed the cost-efficient variant DenseNet-BC [12] which has a growth rate of 12 and three dense blocks each with 16 dense layers, also known as Densenet-BC (k=12, L=100).

In addition, we apply the Global layer to an efficient architecture found by neural architecture search DARTS [22] which uses a cell found by the search. We modify this network by replacing the cell repetitions with a global layer.

Training Details. All the global architectures and their respective original baselines are trained with SGD+momentum optimizer for 300 epochs. We set the initial learning rate to 0.1 and decay by 10 at epoch 150 and 225. Note that for each architecture we use the recommended hyper-parameter settings (batch size, weight decay, data-augmentation etc.). When hyper-parameter recommendations are missing, we use grid search over weight decay $\{3e-4, 2e-4, 1e-4, 5e-5, 1e-5\}$ and batch size $\{32, 64, 128, 256\}$ on a validation set (see Supplementary Sec. A.4 for final hyper-parameters).

Results. We tabulate primary evaluation metrics in the the Table 3. Additional evaluation metrics such as train/inference times and architecture configurations are tabulated in Table 4. Below we summarize the main findings.

(a) Computational and storage savings. Table 3 shows that Global layer enabled architectures are compact and computationally efficient. In comparison to the baseline architectures, models with Global layer achieve $2.5-4.5\times$ flops reduction and $2.5-4.2\times$ parameters reduction.

(b) Lower training and inference times. It is evident from Table 4 that Global architectures have better training and inference times, with at least $2\times$ reductions. Note that we can discard the training time in many IoT applications as a one-time cost. In contrast, the inference time directly affects the battery drain and the responsiveness of the device.

(c) Shallower neural networks. From Table 4, one can deduce that Global architectures are shallower as they reduce the number of cells in the architecture by nearly $3\times$ in many instances. For example, the popular Resnet56 model has 27 cells while Resnet-Global only has 9 cells.

(d) Integrable in many popular architectures. Table 3 and 4 show that Global layer can be successfully applied across a range of architectures with the aforementioned benefits.

(e) Comparison at a fixed computational budget. It is

[2]Following convention [10, 29] we leverage the benchmarked PyTorch utility https://github.com/Lyken17/pytorch-OpCounter for MACs.

Table 3. Results on CIFAR-10 and CIFAR-100. Architectures with Global layer require $2-5\times$ less computational and storage budget.

Architecture	**CIFAR-10**			**CIFAR-100**		
	Accuracy	**Params (Savings)**	**MACs (Savings)**	**Accuracy**	**Params (Savings)**	**MACs (Savings)**
DenseNet-BC [12]	95.49	800K	300M	77.73	800K	300M
Resnet56 [8]	93.03	850K	127M	-	-	
NeuPDE [28]	95.39	9M		76.39	9M	
ANODE [5, 28]	94.96	11M		71.28	11M	
Hamiltonian PDE [24]	89.3	262K		64.9	362K	
MDEQ [2]	93.8	10M	8.3B	-	-	
Resnet32 (m=5)	92.49	460K (1.0×)	70M (1.0×)	68.57	473K (1.0×)	70M (1.0×)
Resnet-Global (m=1)	91.93	162K (2.8×)	15M (4.7×)	68.01	168K (2.8×)	15M (4.7×)
Resnet56 (m=9)	93.03	850K (1.0×)	127M (1.0×)	70.48	861K (1.0×)	127M (1.0×)
Resnet-Global (m=2)	93.01	330K (2.6×)	30M (4.2×)	70.06	336K (2.6×)	30M (4.2×)
Densenet	95.32	769K (1.0×)	297M (1.0×)	77.21	800K (1.0×)	297M (1.0×)
Densenet-Global	95.01	465K (1.7×)	136M (2.2×)	75.69	481K (1.7×)	136M (2.2×)
Wide-Resnet	95.91	9.0M (1.0×)	1.30B (1.0×)	79.11	9.0M (1.0×)	1.30B (1.0×)
Wide-Resnet-Global	95.54	2.8M (3.2×)	425M (3.1×)	78.13	2.8M (3.2×)	427M (3.1×)
DARTS	97.11	3.3M (1.0×)	539M (1.0×)	82.51	3.4M (1.0×)	539M (1.0×)
DARTS-Global	96.83	783K (4.2×)	213M (2.5×)	81.89	835K (4.1×)	213M (2.5×)
Resnet	80.76	13K	3.42M	35.21	14K	3.42M
Resnet-Global	82.55	14K	3.6M	43.62	16K	3.6M
Wide-Resnet	83.83	22K	9.8M	39.01	23K	9.8M
Wide-Resnet-Global	85.51	23K	8.7M	50.23	24K	8.7M
DARTS	86.05	39K	7.7M	54.57	43K	7.7M
DARTS-Global	88.44	34K	8.2M	60.68	41K	8.2M

worth noting that for an IoT device, although storage space could be a prohibitive factor for large models, the main issue with such small devices is computational in nature. The number of floating-point operations used for inference directly impacts the battery drain as well as the real-time latency required for any successful ML application. Keeping this in mind, we compare Global architectures with the baselines under a low computational budget, i.e., $<$ 10M MACs. At this regime, Global models achieve much higher accuracy than the baseline architectures. Thus, demonstrating that our models are better suited for IoT applications.

4.5. Results on Imagenet-1000

Experiments on MNIST and CIFAR datasets demonstrate that architectures with a Global layer are compact, shallower, and computationally efficient. In this section, we show that the Global layer improves the state-of-the-art models for the Imagenet dataset. It has been already shown in the literature that MobileNet [10, 25] and EfficientNet [29] models are more cost-efficient than the Resnet/Densenet models.

Architectures. We apply the global layer to MobileNetV2, MobileNetV3, and EfficientNet and replace the repetitions with the Global layer. For MobileNetV2, we use the baseline with a width multiplier of 1. We obtain MobileNetV2-Global by replacing all the invertible residual block repetitions with one Global layer at each feature resolution. We use the large variant of MobileNetV3 with a width multiplier of 1. We create MobileNetV3-Global by replacing the building block (invertible residual + squeeze-and-excite) with a Global layer. Finally, for the EfficientNet family, we only pick the B0 variant due to its low compute requirements. We provide the architecture details along with building blocks in the Supplementary Sec. A.5.

Training Details. Due to computing limitations, we do not re-train the baselines and only report their publicly known performance metrics in Table 5. We train the architectures with the Global layer from scratch using the hyper-parameter recommendations from the baselines. We use the RMSProp optimizer with 0.9 momentum to minimize the cross-entropy loss along with a weight decay term with a value of $1e-5$. The remaining hyper-parameters are available in the Supplementary Sec. A.5.

Table 4. CIFAR-10: Train & Inference times (cost of one pass through train and test dataset on a V100 GPU) along with the number of cells. Total cells are a proxy for depth of the network.

Architecture	**Accuracy**	**Train Time(s)**	**Inference Time(s)**	**original cells**	**global cells**	**total cells**
Resnet56	93.03	119	6.71	27	0	27
Resnet-Global	93.01	56	2.33	6	3	9
Densenet	95.32	138	10.22	48	0	48
Densenet-Global	95.01	24	3.4	24	2	26
Wide-Resnet	95.91	34	4.88	18	0	18
Wide-Resnet-Global	95.54	20	2.71	3	3	6
DARTS	97.11	126	6.86	20	0	20
DARTS-Global	96.83	61	3.43	6	3	9

Results. Table 5 reports the top1 accuracy along with the number of parameters and number of multiply-add operations. Below we summarize the main findings.

(a) Computational and storage savings. Table 5 shows that Global layer enabled architectures are compact and computationally efficient. Our architectures achieve similar performance as the baselines with $1.5\times$ fewer MACs and $2.5\times$ parameters savings. In addition, with a slight reduction in accuracy, we save $2\times$ MACs and $3\times$ parameters.

(b) Lower training and inference times. Global architectures have better training and inference times, with nearly $2\times$ reductions (see Supplementary Sec. A.5).

(c) Integrable in many popular architectures. Table 5 show that the Global feature layer can be successfully applied across a range of architectures.

Table 5. Results for Imagenet.

Architecture	Imagenet		
	Top-1	#Params	#MACs
MobileNet [11]	70.6	4.2M	575M
SqueezeNext [6]	67.44	3.23M	708M
DenseNet-169 [12]	76.2	14M	3.5B
Resnet-152 [8]	77.8	60M	11B
MDEQ-Small [2]	75.5	18M	
MobileNetV2 [25]	72.0	3.4M $(1.0\times)$	300M $(1.0\times)$
MobileNetV2-Global	71.63	1.6M $(2.1\times)$	193M $(1.6\times)$
MobileNetV2-Global-s	69.03	1.2M $(2.8\times)$	150M $(2.0\times)$
MobileNetV3 [10]	75.2	5.4M $(1.0\times)$	219M $(1.0\times)$
MobileNetV3-Global	74.11	3.0M $(1.8\times)$	156M $(1.4\times)$
MobileNetV3-Global-s	71.89	1.8M $(3.0\times)$	110M $(2.0\times)$
EfficientNet-B0 [29]	77.1	5.3M $(1.0\times)$	390M $(1.0\times)$
EfficientNet-B0-Global	76.12	2.4M $(2.2\times)$	244M $(1.6\times)$
EfficientNet-B0-Global-s	74.53	1.8M $(2.9\times)$	201M $(1.9\times)$

4.6. Ablative Experiments

In this section, we probe various aspects of the proposed method. Due to lack of space, we refer the reader to the Supplementary Sec. A.6 for additional ablations.

(A) Impact of K in iterative solver. We study the effect of the K hyper-parameter in the iterative solver. On CIFAR-10 and CIFAR-100 datasets, Table 6 shows the performance of the Resnet-Global model (see Sec. 4.4) as we vary K. Note that the increasing K does not increase the number of parameters in our formulation. In this case, for CIFAR-10, Resnet-Global has 162K parameters, while for CIFAR-100, Resnet-Global has 168K parameters. Our default choice of $K = 5$ is justifiable from the marginal improvement in accuracy with increased computational cost.

(B) Baseline and Global model with same MACs. Our earlier experiments showed that the Global layer improves the computational footprint of any architecture. In this ablation, we compare the Global architectures with the baselines by keeping the same computational budget. Table 7 shows the performance of these models on the CIFAR-100 dataset. Global models improve baselines by up to 4%.

Table 6. Effect of the hyper-parameter K in update Eq. 4.

Architecture	K	CIFAR-10		CIFAR-100	
		Accuracy	#MACs	Accuracy	#MACs
Resnet-Global	1	90.69	14.3M	66.89	14.3M
Resnet-Global	3	91.34	14.7M	67.37	14.7M
Resnet-Global	5	91.93	15M	68.01	15M
Resnet-Global	10	92.01	15.5M	68.23	15.5M
Resnet-Global	20	92.21	17M	68.24	17M

Table 7. Global models with similar budget as original models.

Architecture	CIFAR-100		
	Accuracy	#Params	#MACs
Resnet56	70.48	861K	127M
Resnet-Global	74.33	1.32M	119M
Densenet	77.21	800K	297M
Densenet-Global	78.91	922K	247M
Wide-Resnet	79.11	9M	1.3B
Wide-Resnet-Global	80.53	9M	1.3B
DARTS	82.51	3.4M	539M
DARTS-Global	84.19	2.4M	519M

(C) Non-linear Residual block as f. We compare the cost of using a standard Residual block as the function f in the update Eq. 4 instead of the identity function. Table 8 shows the performance characteristics of Resnet and WideResnet on CIFAR-10 and CIFAR-100. It shows that using Residual block only brings marginal improvements in accuracy ($< 0.5\%$) with a significant increase in compute cost.

Table 8. Ablative experiments to study the effect of the using a Residual block instead of our current choice in update Eq. 4. Here, all architectures use the Global layer.

Global	Function	CIFAR-10			CIFAR-100		
Architecture	f	Acc.	#Params	#MACs	Acc.	#Params	#MACs
Resnet	Identity	91.93	162K	15M	68.01	168K	15M
Resnet	Residual	92.28	175K	27M	68.37	181K	27M
WideResnet	Identity	95.54	2.8M	425M	78.13	2.8M	427M
WideResnet	Residual	95.67	3M	566M	78.34	3.1M	567M

5. Conclusion

We proposed a novel feature layer that couples the input and output feature map with PDE constraints. The proposed Global layer is readily deployable across many existing architectures. We show that the architectures with Global layers are more compact, shallower, and require less compute for inference and training. Empirical evaluations demonstrate that the proposed layer provides $2-5\times$ storage and computational savings. Since our work reduces model footprint, we do not foresee a negative societal impact.

Acknowledgement

This research was supported by Army Research Office Grant W911NF2110246, the National Science Foundation grants CCF-2007350 and CCF-1955981, ARM Research Inc., and the Hariri Data Science Faculty and Student Fellowship Grants.

References

[1] Shaojie Bai, J. Zico Kolter, and Vladlen Koltun. Deep equilibrium models. In *Advances in Neural Information Processing Systems (NeurIPS)*, 2019. 3

[2] Shaojie Bai, Vladlen Koltun, and J. Zico Kolter. Multiscale deep equilibrium models. 2020. 1, 2, 3, 7, 8

[3] Tian Qi Chen, Yulia Rubanova, Jesse Bettencourt, and David K Duvenaud. Neural ordinary differential equations. In *Advances in Neural Information Processing Systems*, pages 6571–6583, 2018. 1, 2, 5, 6, 12, 13, 15

[4] Emilien Dupont, Arnaud Doucet, and Yee Whye Teh. Augmented neural odes. In H. Wallach, H. Larochelle, A. Beygelzimer, F. d'Alché-Buc, E. Fox, and R. Garnett, editors, *Advances in Neural Information Processing Systems*, volume 32, pages 3140–3150. Curran Associates, Inc., 2019. 2

[5] Amir Gholami, Kurt Keutzer, and George Biros. ANODE: unconditionally accurate memory-efficient gradients for neural odes. *CoRR*, abs/1902.10298, 2019. 1, 2, 7

[6] Amir Gholami, Kiseok Kwon, Bichen Wu, Zizheng Tai, Xiangyu Yue, Peter H. Jin, Sicheng Zhao, and Kurt Keutzer. Squeezenext: Hardware-aware neural network design. *CoRR*, abs/1803.10615, 2018. 2, 8

[7] Song Han, Huizi Mao, and William J Dally. Deep compression: Compressing deep neural networks with pruning, trained quantization and huffman coding. *International Conference on Learning Representations (ICLR)*, 2016. 2

[8] K. He, X. Zhang, S. Ren, and J. Sun. Deep residual learning for image recognition. In *2016 IEEE Conference on Computer Vision and Pattern Recognition (CVPR)*, pages 770–778, 2016. 1, 2, 5, 6, 7, 8, 13, 16

[9] Geoffrey Hinton, Oriol Vinyals, and Jeff Dean. Distilling the knowledge in a neural network. *arXiv preprint arXiv:1503.02531*, 2015. 2

[10] Andrew Howard, Mark Sandler, Grace Chu, Liang-Chieh Chen, Bo Chen, Mingxing Tan, Weijun Wang, Yukun Zhu, Ruoming Pang, Vijay Vasudevan, Quoc V. Le, and Hartwig Adam. Searching for mobilenetv3. *CoRR*, abs/1905.02244, 2019. 5, 6, 7, 8, 14, 15

[11] Andrew G. Howard, Menglong Zhu, Bo Chen, Dmitry Kalenichenko, Weijun Wang, Tobias Weyand, Marco Andreetto, and Hartwig Adam. Mobilenets: Efficient convolutional neural networks for mobile vision applications. *CoRR*, abs/1704.04861, 2017. 2, 8

[12] Gao Huang, Zhuang Liu, Laurens van der Maaten, and Kilian Q. Weinberger. Densely connected convolutional networks. In *Proceedings of the IEEE Conference on Computer Vision and Pattern Recognition (CVPR)*, July 2017. 2, 5, 6, 7, 8, 13

[13] G D Hutomo, J Kusuma, A Ribal, A G Mahie, and N Aris. Numerical solution of 2-d advection-diffusion equation with variable coefficient using du-fort frankel method. 1180:012009, feb 2019. 4, 12

[14] Forrest N. Iandola, Matthew W. Moskewicz, Khalid Ashraf, Song Han, William J. Dally, and Kurt Keutzer. Squeezenet: Alexnet-level accuracy with 50x fewer parameters and <1mb model size. *CoRR*, abs/1602.07360, 2016. 2

[15] Anil Kag and Venkatesh Saligrama. Time adaptive recurrent neural network. In *Proceedings of the IEEE/CVF Conference on Computer Vision and Pattern Recognition (CVPR)*, pages 15149–15158, June 2021. 3

[16] Anil Kag and Venkatesh Saligrama. Training recurrent neural networks via forward propagation through time. In Marina Meila and Tong Zhang, editors, *Proceedings of the 38th International Conference on Machine Learning*, volume 139 of *Proceedings of Machine Learning Research*, pages 5189–5200. PMLR, 18–24 Jul 2021. 17

[17] Anil Kag, Ziming Zhang, and Venkatesh Saligrama. Rnns incrementally evolving on an equilibrium manifold: A panacea for vanishing and exploding gradients? In *International Conference on Learning Representations*, 2020. 3

[18] Alex Krizhevsky. Learning multiple layers of features from tiny images. Technical report, 2009. 5

[19] Alex Krizhevsky, Ilya Sutskever, and Geoffrey E Hinton. Imagenet classification with deep convolutional neural networks. In F. Pereira, C. J. C. Burges, L. Bottou, and K. Q. Weinberger, editors, *Advances in Neural Information Processing Systems*, volume 25, pages 1097–1105. Curran Associates, Inc., 2012. 1, 2

[20] Yann LeCun, Corinna Cortes, and CJ Burges. Mnist handwritten digit database. *ATT Labs [Online]. Available: http://yann.lecun.com/exdb/mnist*, 2, 2010. 5

[21] Chenxi Liu, Barret Zoph, Jonathon Shlens, Wei Hua, Li-Jia Li, Li Fei-Fei, Alan L. Yuille, Jonathan Huang, and Kevin Murphy. Progressive neural architecture search. *CoRR*, abs/1712.00559, 2017. 2

[22] Hanxiao Liu, Karen Simonyan, and Yiming Yang. DARTS: Differentiable architecture search. In *International Conference on Learning Representations*, 2019. 5, 6, 13, 14, 17

[23] Olga Russakovsky, Jia Deng, Hao Su, Jonathan Krause, Sanjeev Satheesh, Sean Ma, Zhiheng Huang, Andrej Karpathy, Aditya Khosla, Michael Bernstein, Alexander C. Berg, and Li Fei-Fei. ImageNet Large Scale Visual Recognition Challenge. *International Journal of Computer Vision (IJCV)*, 115(3):211–252, 2015. 5

[24] Lars Ruthotto and Eldad Haber. Deep neural networks motivated by partial differential equations, 2018. 3, 5, 7

[25] Mark Sandler, Andrew Howard, Menglong Zhu, Andrey Zhmoginov, and Liang-Chieh Chen. Mobilenetv2: Inverted residuals and linear bottlenecks. In *Proceedings of the IEEE Conference on Computer Vision and Pattern Recognition (CVPR)*, June 2018. 7, 8, 14

[26] Karen Simonyan and Andrew Zisserman. Very deep convolutional networks for large-scale image recognition. In *International Conference on Learning Representations*, 2015. 2

[27] Rupesh Kumar Srivastava, Klaus Greff, and Jürgen Schmidhuber. Highway networks. *CoRR*, abs/1505.00387, 2015. 2

[28] Yifan Sun, Linan Zhang, and Hayden Schaeffer. NeuPDE: Neural network based ordinary and partial differential equations for modeling time-dependent data. In Jianfeng Lu and Rachel Ward, editors, *Proceedings of The First Mathematical and Scientific Machine Learning Conference*, volume 107 of

Proceedings of Machine Learning Research, pages 352–372, Princeton University, Princeton, NJ, USA, 20–24 Jul 2020. PMLR. 3, 5, 6, 7, 12, 13

[29] Mingxing Tan and Quoc Le. EfficientNet: Rethinking model scaling for convolutional neural networks. In Kamalika Chaudhuri and Ruslan Salakhutdinov, editors, *Proceedings of the 36th International Conference on Machine Learning*, volume 97 of *Proceedings of Machine Learning Research*, pages 6105–6114, Long Beach, California, USA, 09–15 Jun 2019. PMLR. 2, 5, 6, 7, 8, 15

[30] Trieu Trinh, Andrew Dai, Thang Luong, and Quoc Le. Learning longer-term dependencies in RNNs with auxiliary losses. In Jennifer Dy and Andreas Krause, editors, *Proceedings of the 35th International Conference on Machine Learning*, volume 80 of *Proceedings of Machine Learning Research*, pages 4965–4974. PMLR, 10–15 Jul 2018. 17

[31] Yaqing Wang, Quanming Yao, James Kwok, and Lionel M. Ni. Generalizing from a few examples: A survey on few-shot learning, 2020. 1

[32] Sergey Zagoruyko and Nikos Komodakis. Wide residual networks. In *BMVC*, 2016. 2, 5, 6, 13

[33] Zhong-Qiu Zhao, Peng Zheng, Shou tao Xu, and Xindong Wu. Object detection with deep learning: A review, 2019. 1

[34] Barret Zoph and Quoc V. Le. Neural architecture search with reinforcement learning. *CoRR*, abs/1611.01578, 2016. 2